9th IEEE-RAS International Conference on Humanoid Robots
December 7-10, 2009 Paris, France

Effect of Foot Shape on Locomotion of Active Biped Robots

Katsu Yamane*† and Laura Trutoiu†
*Disney Research, Pittsburgh †Carnegie Mellon University
Email: kyamane@disneyresearch.com

Abstract— **This paper investigates the effect of foot shape on biped locomotion. In particular, we consider planar biped robots whose feet are composed of curved surfaces at toe and heel and a flat section between them. We developed an algorithm that can optimize the gait pattern for a set of foot shape, walk speed and step length. The optimization is formulated based on the rigid-body and collision dynamics of the robot model and tries to minimize the ankle torque. We also divide a step into two phases at collision events and optimize each phase separately with appropriate boundary conditions. Numerical experiments using walk parameters from human motion capture data suggest that having a curved toe and heel would be a way to realize locomotion at speeds comparable to human.**

I. Introduction

Walking is one of the most common whole-body motions for humans, and biped robots with locomotion capability are not uncommon these days. However, it is still challenging to realize locomotion comparable to human in terms of efficiency, speed, robustness, adaptability and smoothness.

A typical approach to realize active dynamic walking is to first generate a physically feasible joint pattern based on a simplified robot model and predefined foot trajectories, and then apply a joint servo controller to track the generated pattern. A balance controller is usually added to maintain balance under modeling errors and disturbances. Using this approach, researchers have realized locomotion in various environments including rough terrains [1] and stairs [2]. However, the gaits tend to be less efficient compared to human locomotion because of the high gains used to track the trajectory. In addition, the locomotion style is typically very different from human because the knee joints are bent to increase the robustness and the feet are maintained parallel to the ground to make balancing easier.

The passive walking community, on the other hand, has successfully achieved efficient locomotion with passive biped robots [3]. Although their approach is a promising way towards better robot locomotion, it cannot be applied to general-purpose humanoid robots directly because of the low adaptability to different environments or walk parameters.

The motivation of this work is to achieve graceful and efficient motions for humanoid robots. In addition to the mechanical design and control algorithm, the external body geometry would also have a large impact on the overall motion quality because humanoid robots physically interact with the environment through contacts. In particular, the feet make the most frequent interaction with the environment and their shape affects many important behaviors including walking and running.

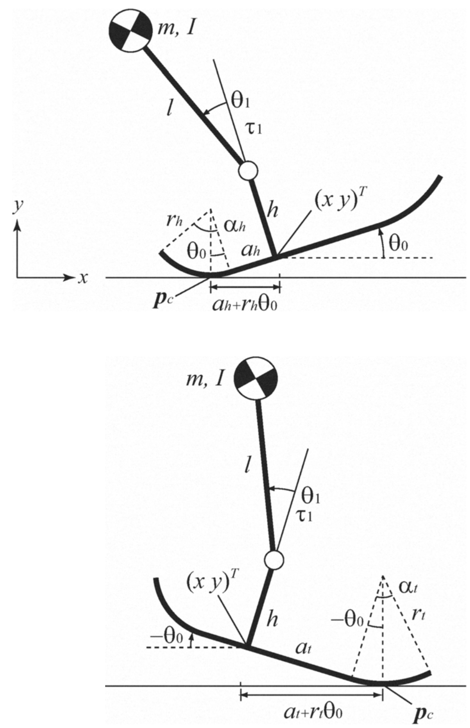

Fig. 1. The foot model used in our analysis.

In this paper, we investigate the effect of foot sole shape on the locomotion of planar active biped robots, inspired by the use of circular feet in some of the work in passive walking [3]. More specifically, we consider a foot composed of two curved sections at the toe and heel, connected by a flat section between them (Fig. 1). For a set of foot shape, walking speed and step length, our optimization algorithm calculates the gait pattern on horizontal ground that minimizes the ankle torque. The optimization is based on the rigid-body and collision dynamics of the simplified biped model with a rigid body, ankle joints, and feet. Because each step involves two collisions that introduce discontinuity not handled by the solver, we divide a step into two phases and optimize each phase separately with appropriate boundary conditions derived from the collision dynamics.

The numerical experiments using gait parameters from human motion capture data suggest that having curved toe and heel would be a way to realize locomotion at speeds comparable to human. We also observe that ankle joint torques are reduced by using curved feet.

II. Related Work

Several different foot shapes have been investigated in the literature for both active and passive walking. While most of the current humanoid robot feet have rectangular flat surfaces to provide good standing balance [4]–[6], some robots are equipped with active [7], [8] or passive [9]–[11] toe joints, mostly to increase step length and decrease knee joint loads. It is also shown that active toe joints can reduce the energy consumption [12]. Most of these toe mechanisms, as well as feet with curved toe and heel similar to the one used in the paper, have already been proposed by Nishiwaki et al. [13]. In particular, they proposed to design the toe and heel curvature so that the ankle joint follows a predefined trajectory to increase the walking speed. However, the efficiency and robustness issues still remain because the main approaches to locomotion pattern generation and control are essentially the same.

Because human feet have fairly complex geometry and mechanism, it is also interesting to understand the reason of having such complexity through human biomechanics. In fact, several studies have shown the advantages of the curved, flexible sole in humans, such as less metabolic cost for arcs with larger radius [14].

Foot shape and mechanism are one of the key design issues in passive walking robots [3], [15] that typically have no or minimal actuators and controllers and realize low energy costs as well as human-like gait patterns. Their feet typically have curved shapes [3], [15] or flat shape with torsional spring at the ankles [16]. In curved feet, the radius of the curve is usually chosen to be equal to the height of the center of mass so that the robot emulates the motion of a wheel rolling down a slope. These shapes result in more efficient gaits because the primary energy loss in biped walking is due to dissipation at the foot.

Gait generation for passive walkers relies on the existence of initial conditions that result in cyclic patterns for the step to step transition function. Finding a cycle pattern reduces to a root finding problem and can be solved either through numerical solutions, theoretical models or intuition based on previous solutions [17]. However, it is usually difficult to generate gaits for arbitrary walk parameters, or to optimize the robot design.

III. The Biped Model

A. Foot and Leg

We consider a foot with circular segments at the toe and heel, connected by a flat section in the middle. This choice is inspired by some of the prior work including the circular feet used in passive walking robots and passive toe joints used in some fully-actuated biped robots. The curved toe and heel parts have a similar effect to adding a passive joint because the ground reaction torque around the toe will be proportional to the angle of the foot with respect to the ground.

We represent the mass of the entire robot as a single rigid body with mass m and inertia I. Each leg has one joint at the ankle but no knee joint. The rationale behind not having a knee joint is that the knee joint is likely to be locked at the joint limit in the supporting leg, and the knee joint torque is always zero in the free leg because we ignore the mass of the foot and leg.

The variables used in the rest of the paper are summarized in Fig. 1 and reviewed in the rest of this section.

B. Kinematics

The configuration of a single leg is fully determined by four parameters: (x, y) representing the position of the point fixed to the foot, θ_0 representing the angle of the flat part with respect to the horizontal ground, and θ_1 representing the ankle joint angle.

We define the following vectors to describe the configuration of the leg:

$$\boldsymbol{q} = \begin{pmatrix} x & y & \theta_0 & \theta_1 \end{pmatrix}^T \tag{1}$$

$$\boldsymbol{p} = \begin{pmatrix} x & y \end{pmatrix}^T \tag{2}$$

and to describe the forces/torques applied to the leg:

$$\boldsymbol{\tau} = \begin{pmatrix} f_x & f_y & \tau_0 & \tau_1 \end{pmatrix}^T. \tag{3}$$

We will also use these shorthands to simplify the equations:

$$\begin{aligned} c_* &= \cos\theta_* \\ s_* &= \sin\theta_* \\ c_{01} &= \cos(\theta_0 + \theta_1) \\ s_{01} &= \sin(\theta_0 + \theta_1) \\ H_1 &= h^2 + l^2 + 2hlc_1 \\ L_1 &= l^2 + hlc_1 \\ A_{01} &= hc_0 + lc_{01} \\ B_{01} &= hs_0 + ls_{01}. \end{aligned}$$

The position and velocity of the mass can be written as

$$\boldsymbol{p}_m = \begin{pmatrix} x_m \\ y_m \end{pmatrix} = \begin{pmatrix} x - B_{01} \\ y + A_{01} \end{pmatrix} \tag{4}$$

$$\dot{\boldsymbol{p}}_m = \begin{pmatrix} \dot{x} - A_{01}\dot{\theta}_0 - lc_{01}\dot{\theta}_1 \\ \dot{y} - B_{01}\dot{\theta}_0 - ls_{01}\dot{\theta}_1 \end{pmatrix} \tag{5}$$

and the Jacobian matrix of $\boldsymbol{p}_m$ with respect to the joint variables is

$$\boldsymbol{J}_m = \frac{\partial \boldsymbol{p}_m}{\partial \boldsymbol{q}} = \begin{pmatrix} 1 & 0 & -A_{01} & -lc_{01} \\ 0 & 1 & -B_{01} & -ls_{01} \end{pmatrix}. \tag{6}$$

C. Contact Constraints

If a foot is in contact with a flat surface, we can uniquely determine the leg configuration by θ_0 and θ_1. The following paragraphs detail the expression of foot position and contact point position for heel and toe contacts, assuming that the surface is horizontal and represented as $y = 0$.

a) Heel Contact: If $\theta_0 > 0$, the foot makes heel contact as shown in the top figure of Fig. 1. The position, velocities and accelerations of the foot can be determined by

$$\begin{aligned} \boldsymbol{p} &= \begin{pmatrix} nL - a_h - r_h\theta_0 + r_h s_0 + a_h c_0 \\ r_h - r_h c_0 + a_h s_0 \end{pmatrix} \\ \dot{\boldsymbol{p}} &= \begin{pmatrix} (-r_h + r_h c_0 - a_h s_0)\dot{\theta}_0 \\ (r_h s_0 + a_h c_0)\dot{\theta}_0 \end{pmatrix} \\ \ddot{\boldsymbol{p}} &= \begin{pmatrix} (-r_h + r_h c_0 - a_h s_0)\ddot{\theta}_0 + (-r_h s_0 - a_h c_0)\dot{\theta}_0^2 \\ (r_h s_0 + a_h c_0)\ddot{\theta}_0 + (r_h c_0 - a_h s_0)\dot{\theta}_0^2 \end{pmatrix} \end{aligned}$$

respectively, where L is the step length and $n \geq 0$ represents the number of steps taken.

The contact point position and velocity can be calculated as follows:

$$\begin{aligned} \boldsymbol{p}_c = \begin{pmatrix} x_c \\ y_c \end{pmatrix} &= \begin{pmatrix} x - r_h s_0 - a_h c_0 \\ y - r_h + r_h c_0 - a_h s_0 \end{pmatrix} \\ \dot{\boldsymbol{p}}_c = \begin{pmatrix} \dot{x}_c \\ \dot{y}_c \end{pmatrix} &= \begin{pmatrix} \dot{x} + (-r_h c_0 + a_h s_0)\dot{\theta}_0 \\ \dot{y} + (-r_h s_0 - a_h c_0)\dot{\theta}_0 \end{pmatrix}. \end{aligned}$$

We can also derive the Jacobian matrix of the contact point position with respect to joint variables as follows:

$$\boldsymbol{J}_c = \frac{\partial \boldsymbol{p}_c}{\partial \boldsymbol{q}} = \begin{pmatrix} 1 & 0 & -r_h c_0 + a_h s_0 & 0 \\ 0 & 1 & -r_h s_0 - a_h c_0 & 0 \end{pmatrix}. \tag{7}$$

b) Toe Contact: If $\theta_0 < 0$, the foot makes heel contact as shown in the bottom figure of Fig. 1. The expressions corresponding to the heel contact case are as follows:

$$\begin{aligned} \boldsymbol{p} &= \begin{pmatrix} nL + a_t - r_t\theta_0 + r_t s_0 - a_t c_0 \\ r_t - r_t c_0 - a_t s_0 \end{pmatrix} \\ \dot{\boldsymbol{p}} &= \begin{pmatrix} (-r_t + r_t c_0 + a_t s_0)\dot{\theta}_0 \\ (r_t s_0 - a_t c_0)\dot{\theta}_0 \end{pmatrix} \\ \ddot{\boldsymbol{p}} &= \begin{pmatrix} (-r_t + r_t c_0 + a_t s_0)\ddot{\theta}_0 + (-r_t s_0 + a_t c_0)\dot{\theta}_0^2 \\ (r_t s_0 - a_t c_0)\ddot{\theta}_0 + (r_t c_0 + a_t s_0)\dot{\theta}_0^2 \end{pmatrix} \end{aligned}$$

$$\begin{aligned} \boldsymbol{p}_c = \begin{pmatrix} x_c \\ y_c \end{pmatrix} &= \begin{pmatrix} x - r_t s_0 + a_t c_0 \\ y - r_t + r_t c_0 + a_t s_0 \end{pmatrix} \\ \dot{\boldsymbol{p}}_c = \begin{pmatrix} \dot{x}_c \\ \dot{y}_c \end{pmatrix} &= \begin{pmatrix} \dot{x} + (-r_t c_0 - a_t s_0)\dot{\theta}_0 \\ \dot{y} + (-r_t s_0 + a_t c_0)\dot{\theta}_0 \end{pmatrix} \end{aligned}$$

$$\boldsymbol{J}_c = \frac{\partial \boldsymbol{p}_c}{\partial \boldsymbol{q}} = \begin{pmatrix} 1 & 0 & -r_t c_0 - a_t s_0 & 0 \\ 0 & 1 & -r_t s_0 - a_t c_0 & 0 \end{pmatrix}. \tag{8}$$

D. Dynamics

Using Lagrange's equation of motion, we can derive the equation of motion of a single leg in the following form:

$$\boldsymbol{\tau} = \boldsymbol{M}\ddot{\boldsymbol{q}} + \boldsymbol{c} + \boldsymbol{g} \tag{9}$$

where

$$\boldsymbol{M} = \begin{pmatrix} m & 0 & -mA_{01} & -mlc_{01} \\ 0 & m & -mB_{01} & -mls_{01} \\ -mA_{01} & -mB_{01} & mH_1 + I & mL_1 \\ -mlc_{01} & -mls_{01} & mL_1 & ml^2 + I \end{pmatrix} \tag{10}$$

$$\boldsymbol{c} = m \begin{pmatrix} B_{01}\dot{\theta}_0^2 + 2ls_{01}\dot{\theta}_0\dot{\theta}_1 + ls_{01}\dot{\theta}_1^2 \\ -A_{01}\dot{\theta}_0^2 - 2lc_{01}\dot{\theta}_0\dot{\theta}_1 - lc_{01}\dot{\theta}_1^2 \\ -2hls_1\dot{\theta}_0\dot{\theta}_1 - hls_1\dot{\theta}_1^2 \\ hls_1\dot{\theta}_0^2 \end{pmatrix} \tag{11}$$

$$\boldsymbol{g} = mg \begin{pmatrix} 0 \\ 1 \\ -B_{01} \\ -ls_{01} \end{pmatrix}. \tag{12}$$

Because the system is underactuated, not all combinations of $\ddot{\theta}_0$ and $\ddot{\theta}_1$ are physically feasible at a particular state. We use $\Delta\tau$, the torque around the contact point required to realize the given $\ddot{\theta}_0$ and $\ddot{\theta}_1$, as the measure of physical infeasibility of the motion because the point contacts at heel and toe cannot provide $\Delta\tau$. We can calculate $\Delta\tau$ by first computing $\boldsymbol{\tau}$ using Eq.(9) and then computing the equivalent torque around the contact point by

$$\Delta\tau = \tau_0 + (y_c - y)f_x - (x_c - x)f_y \tag{13}$$

in the toe or heel contact case. If the foot is in flat contact, i.e. $\theta_0 = 0$, the motion is physically feasible if the center of pressure is in the flat section of the foot. $\Delta\tau$ therefore becomes

$$\Delta\tau = \begin{cases} \tau_0 - a_t f_y & \text{if } \tau_0 - a_t f_y > 0 \\ \tau_0 + a_h f_y & \text{if } \tau_0 + a_h f_y < 0 \\ 0 & \text{otherwise.} \end{cases} \tag{14}$$

E. Collisions

There are two types of collisions in each walk cycle of our foot model: a) a swing leg makes a new contact with the ground, and b) a foot already in contact transitions to flat contact. We assume that all collisions are completely rigid and inelastic, i.e. the foot and ground do not deform and the velocity of the colliding point turns to zero after the collision. The purpose of having collision models is to derive the boundary conditions for the optimization because we divide a walk cycle into two phases and optimize each phase separately, as described in the next section.

We first derive the equations for collision a). Figure 2 depicts a typical configuration when this type of collision occurs, where the colliding leg is drawn by dashed lines. In the following equations, the variables with ^ represent the quantities associated with the supporting leg. We assume that the supporting leg leaves the ground immediately after the collision. Therefore, only one impulse at the colliding foot denoted $\boldsymbol{F}$ is involved in the collision. The conservation of momentum is written as follows:

$$\boldsymbol{M}\dot{\boldsymbol{q}}^- + \boldsymbol{J}_c^T\boldsymbol{F} = \boldsymbol{M}\dot{\boldsymbol{q}}^+ \tag{15}$$

where $\dot{\boldsymbol{q}}^-$ and $\dot{\boldsymbol{q}}^+$ are the joint velocities before and after the collision. We also have to consider the kinematic constraint where the velocity of the center of mass must match between supporting and colliding legs. This constraint is written as

$$\boldsymbol{J}_m\dot{\boldsymbol{q}}^- = \hat{\boldsymbol{J}}_m\dot{\hat{\boldsymbol{q}}}^-. \tag{16}$$

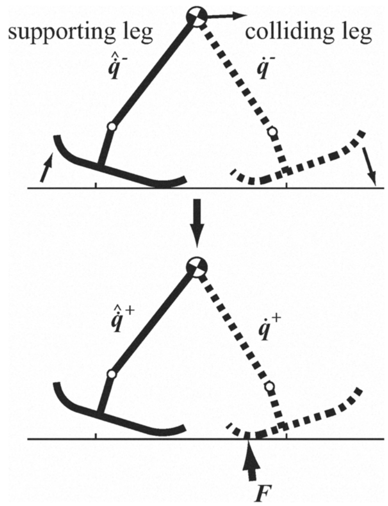

Fig. 2. Collision a): swing leg collision.

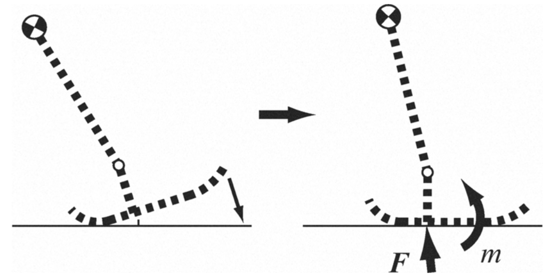

Fig. 3. Collision b): Foot making flat contact.

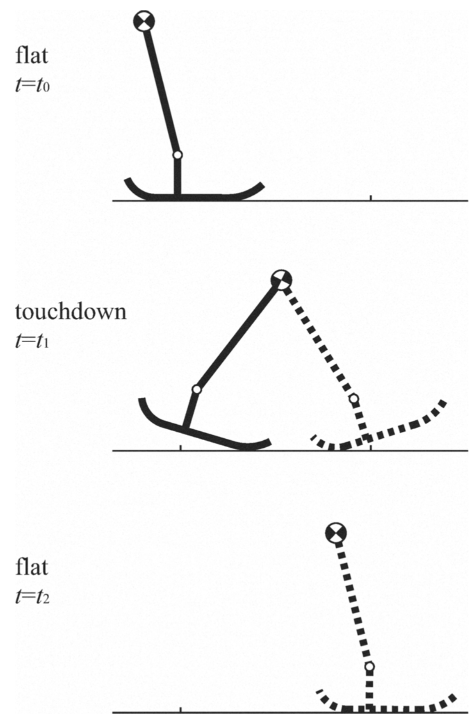

Fig. 4. Three events during a step.

We divide a step into two phases at the touchdown and optimize each phase separately (the optimization process will be detailed in the next section). Therefore, our interest here is if we can optimize $\hat{\dot{\boldsymbol{q}}}^-$ and $\dot{\boldsymbol{q}}^+$ independently. For any given pair of $\hat{\dot{\boldsymbol{q}}}^-$ and $\dot{\boldsymbol{q}}^+$, we can obtain $\boldsymbol{F}$ by solving the linear equation

$$\left(\boldsymbol{J}_m \boldsymbol{M}^{-1} \boldsymbol{J}_c^T\right) \boldsymbol{F} = \boldsymbol{J}_m \dot{\boldsymbol{q}}^+ - \hat{\boldsymbol{J}}_m \hat{\dot{\boldsymbol{q}}}^-, \tag{17}$$

which is obtained by eliminating $\dot{\boldsymbol{q}}^-$ from Eqs.(15) and (16). Once we obtain $\boldsymbol{F}$, we can compute $\dot{\boldsymbol{q}}^-$ by

$$\dot{\boldsymbol{q}}^- = \dot{\boldsymbol{q}}^+ - \boldsymbol{M}^{-1} \boldsymbol{J}_c^T \boldsymbol{F} \tag{18}$$

which suggests that we can realize any $\dot{\boldsymbol{q}}^+$ by adjusting the velocity of the swing leg before collision, and therefore we do not have to enforce any boundary condition at this collision.

Collision b) is formulated as (see Fig. 3)

$$\begin{aligned} \boldsymbol{M}\dot{\boldsymbol{q}}^- + \boldsymbol{J}_f^T \boldsymbol{H} &= \boldsymbol{M}\dot{\boldsymbol{q}}^+ & (19)\\ \boldsymbol{J}_f \dot{\boldsymbol{q}}^+ &= \boldsymbol{0} & (20) \end{aligned}$$

where $\boldsymbol{H} = \left(\boldsymbol{F}^T \ m\right)^T$ is the impulse force and moment applied to the foot link and

$$\boldsymbol{J}_f = \begin{pmatrix} 1 & 0 & 0 & 0 \\ 0 & 1 & 0 & 0 \\ 0 & 0 & 1 & 0 \end{pmatrix}. \tag{21}$$

We can obtain $\boldsymbol{H}$ by

$$\boldsymbol{H} = -\left(\boldsymbol{J}_f \boldsymbol{M}^{-1} \boldsymbol{J}_f^T\right)^{-1} \boldsymbol{J}_f \dot{\boldsymbol{q}}^-. \tag{22}$$

However, because all elements in the last row of $\boldsymbol{J}_f^T$ are zero, the last elements of $\boldsymbol{M}\dot{\boldsymbol{q}}^-$ and $\boldsymbol{M}\dot{\boldsymbol{q}}^+$ must be equal. As described in the next section, we first sample $\dot{\boldsymbol{q}}^+$ in our optimization. We therefore add the boundary condition $\boldsymbol{m}_1 \dot{\boldsymbol{q}}^- = \boldsymbol{m}_1 \dot{\boldsymbol{q}}^+$ in the optimization responsible for the part before this collision, where $\boldsymbol{m}_1$ denotes the bottom row of $\boldsymbol{M}$.

IV. Gait Optimization

A. Representation of a Gait

Figure 4 depicts the three events that occur during each step of locomotion. The start of a step $(t = t_0)$ is defined as the moment when the supporting leg makes flat contact with the floor. The swing leg then makes a touchdown at $t = t_1$, followed by its flat contact at $t = t_2$.

We divide a step into two phases: *Phase 1* (from flat contact to touchdown) and *Phase 2* (from touchdown to flat contact). Due to the discontinuity at the touchdown, the two phases have to be optimized separately with the following three boundary conditions:

- The swing and colliding legs must share the mass position at $t = t_1$.
- The configurations at $t = t_0$ and $t = t_2$ must be the same.
- The velocity at the end of *Phase 2* must satisfy the collision boundary condition.

TABLE I

INITIAL AND FINAL VALUES FOR θ_0 AND θ_1 IN EACH PHASE.

time	t_0	t_1	t_2
θ_0	0	sampled	0
$\dot{\theta}_0$	0	optimized	optimized
θ_1	given	sampled	given
$\dot{\theta}_1$	given	optimized	optimized

As shown in Section III, the configuration of the biped robot is fully determined by θ_0 and θ_1 due to the contact constraints. We therefore represent the motion by two spline curves for each phase representing the trajectories of θ_0 and θ_1, and obtain the knot points that minimize the cost function described in the next subsection.

B. Optimizing the Whole Gait

Table I summarizes how the initial and final states are given for each phase. Because of the inelastic collision assumption, we have $\theta_0(t_0) = \theta_0(t_2) = 0$ and $\dot{\theta}_0(t_0) = 0$. For simplicity, we consider the case where the rest of the initial states, i.e. $\theta_1(t_0) = \theta_1(t_2)$ and $\dot{\theta}_1(t_0)$, are also given. The joint angles at t_1 are sampled and the best sample is chosen after optimizing the gait for each sample. The joint velocities will be obtained as a result of the optimization.

We obtain the optimal gait for the given initial state at $t = t_0$ by the following steps:

1) Sample $\theta_0(t_1)$ and $\theta_1(t_1)$.
2) Obtain the optimal gait (represented by joint trajectories) for each sample.
3) Find the gait with the lowest cost among the trajectories obtained in step 2).

Step 2) is further divided into the following three steps:

2-1. For *Phase 1*, repeat:
  - Randomly sample knot points for θ_0 and θ_1.
  - Optimize the knot points using a gradient-based algorithm.

2-2. Perform the same process for *Phase 2*.

2-3. Among all pairs of trajectories from *Phase 1* and *Phase 2*, find the pair with the minimum total cost.

In the following subsection, we describe how to optimize the joint trajectories for each phase (steps 2-1 and 2-2).

C. Optimizing a Single Phase

We first randomly sample the knot points for θ_0 and θ_1. A sample is drawn by first computing a K-element array a_i $(i = 1, \dots, K)$ by $a_1 = 0$, $a_i = a_{i-1} + r(0, 1)$ $(i = 2, \dots, K)$ where K is the number of knot points and $r(s, t)$ is a function that returns a random number between s and t, and then scaling and shifting a_i to satisfy the joint angle boundary conditions. We then fit the trajectories of θ_0 and θ_1 by piece-wise third-order polynomials that pass through the knot points and satisfy the boundary conditions for the velocity.

We chose to minimize the sum of squared ankle torques in our optimization, although there are a number of criteria proposed for evaluating biped locomotion. We also have to consider the physical feasibility of the motion because we simply represent the joint trajectories by two independent spline interpolations for θ_0 and θ_1. Therefore, we also include $\Delta\tau$ defined in Section III-D to maximize the physical consistency of the resulting motion.

TABLE II

MODEL PARAMETERS USED IN THE NUMERICAL EXPERIMENTS.

	Flat	*Curved 1*	*Curved 2*	*Curved 3*
m (kg)	60			
I (kgm^2/s)	1.0			
h (m)	0.1			
l (m)	0.7			
max/min θ_0 (rad)	-0.5/0.5			
max/min θ_1 (rad)	-0.8/0.8			
r_h (m)	0.001	0.05	0.1	0.15
α_h (rad)	0.5	0.5	0.5	0.5
a_h (m)	0.0995	0.075	0.05	0.025
r_t (m)	0.001	0.1	0.2	0.3
α_t (rad)	0.5	0.5	0.5	0.5
a_t (m)	0.1995	0.15	0.1	0.05
shape	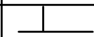	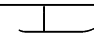	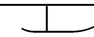	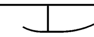

The cost function to be minimized is

$$Z = \frac{1}{2}\sum \tau_1^2 + \frac{w}{2}\sum \Delta\tau^2 \tag{23}$$

where w is a constant weight. We compute the partial derivative of the cost function with respect to the knot positions, and apply the conjugate gradient method to obtain the optimal knot points.

V. RESULTS

A. Setup

We chose three foot models with different radii for the curved section and calculated the optimal locomotion pattern for each model. Table II summarizes the model parameters used for the experiments. The parameters were chosen so that the total length of the foot is constant for all models (0.1 m for the heel side and 0.2 m for the toe side). The maximum and minimum values of θ_0 to make contact at the circular sections were also the same for all models.

We used the gait parameters shown in Table III. The parameters were extracted from motion capture clips of walking motions with three different speeds randomly selected from a human motion capture database [18]. The joint angles of the supporting leg at the end of *Phase 1* were sampled from a uniform grid in the θ_0–θ_1 space with the intervals of 0.05 rad for $-0.5 \le \theta_0 \le 0$ and 0.08 rad for $-0.8 \le \theta_1 \le 0.8$. Note that θ_0 must be negative to make toe contact. The total number of grid points is 231.

The trajectories of θ_0 and θ_1 were represented by a spline curve with five knot points including the start and end points. We started the optimization from 100 random initial knot points for each sample. The weight parameter for the optimization was $w = 10$. We used larger weights for the physical constraints to make the resulting motion as physically consistent as possible.

TABLE III

GAIT PARAMETERS.

	slow	normal	fast
step length (m)	0.94	0.96	0.99
Phase 1 duration (s)	0.83	0.46	0.31
Phase 2 duration (s)	0.17	0.14	0.08
body velocity (m/s)	0.62	0.94	1.26

B. Results

Table IV summarizes the numerical optimization results. Although we sampled 231 points for the touchdown joint angles, the number of gaits may be smaller because not all of the samples have valid inverse kinematics solution for the touchdown leg. In addition, we rejected the optimization result if any of the joint angles exceed their motion range. We did not impose joint velocity, acceleration or torque limits.

We observe that there is a large variation in the number of gaits obtained for the combinations. All foot shapes had a number of possible gaits for slow walk, while some foot shapes did not have a gait for normal and fast walk. In general, it was easier to find a gait for the curved feet.

The foot angle (θ_0) of the supporting leg at touchdown also varied across walk speed and foot shapes. Most foot shapes achieved slow walk keeping the supporting foot flat, with the exception of *Curved 3* feet that showed slight toe contact. The optimal gaits for both normal and fast walks had significant toe contact phase except for the only solution for the *Flat* feet. The squared ankle torque was also smaller with curved feet by 12–21%.

Figure 5 shows the stick figure representations of the optimal gaits obtained for each combination of walk speed and foot shape.

Figure 6 shows the vertical contact force during the fast walk by *Curved 3* foot. The time axis is adjusted so that the touchdown becomes $t = 0$. It is known in biomechanics [19] that the contact force during human walking has two peaks at the beginning and end of the contact. The contact force of the optimized gait pattern shows similar tendency, except for the impulsive force at the beginning due to the rigid, inelastic collision model.

VI. CONCLUSION

In this paper, we investigated the effect of foot shape on biped locomotion. We focused on a foot shape with circular sections in the toe and heel and a flat section between them, and obtained optimal walk patterns for given foot shapes and walk parameters using a numerical optimization technique. The optimization is based on the rigid-body and collision dynamics of the simplified leg model. We also divided a step into two phases to allow discontinuity at collisions.

Comparison with flat feet and curved feet with three radii sets suggested that having curved feet would be a way to realize walking at speeds comparable to the human. Even in cases where the optimization could not find a gait for flat feet, it was able to find one or more gaits for curved feet. In addition, optimal gaits for curved feet utilize toe contact

TABLE IV

RESULT SUMMARY. $\sharp$: NUMBER OF GAITS FOUND, (θ_0, θ_1): THE JOINT ANGLES OF THE SUPPORTING LEG AT TOUCHDOWN FOR THE MINIMUM-TORQUE GAIT, $\int \tau_1^2 dt$: SQUARED ANKLE TORQUE INTEGRATED OVER A STEP.

gait	foot	$\sharp$	(θ_0, θ_1)	$\int \tau_1^2 dt$
slow	*Flat*	11	(0, -0.64)	1.85×10^4
	Curved 1	12	(0, -0.64)	1.53×10^4
	Curved 2	11	(0, -0.72)	1.46×10^4
	Curved 3	8	(-0.1, -0.56)	1.62×10^4
normal	*Flat*	1	(0, -0.72)	1.57×10^4
	Curved 1	0	–	–
	Curved 2	9	(-0.45, -0.24)	1.31×10^4
	Curved 3	10	(-0.45, -0.24)	1.30×10^4
fast	*Flat*	0	–	–
	Curved 1	0	–	–
	Curved 2	1	(-0.4, -0.32)	9.57×10^3
	Curved 3	4	(-0.4, -0.32)	9.51×10^3

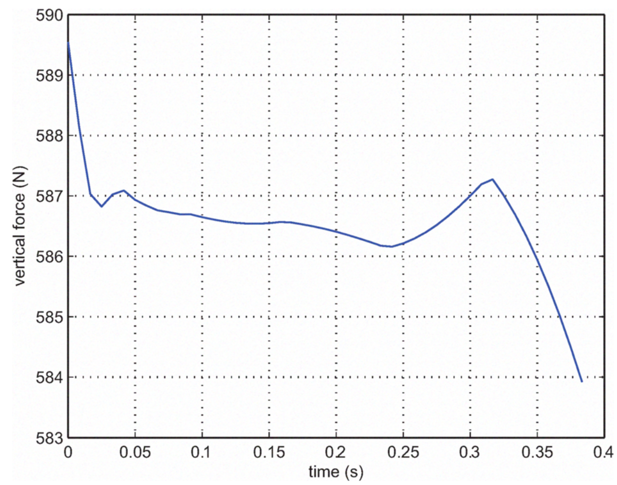

Fig. 6. Vertical contact force in the fast walk by *Curved 3*.

of the supporting leg. They also require smaller ankle torque than flat feet.

This is our first trial to evaluate the effect of curved feet for active biped robots on locomotion. It would be interesting to consider more general shapes and/or add passive elements to the foot. Optimization of the shape, rather than the gait, is also an interesting research direction. One of the possible drawbacks of using toe and heel contacts is the difficulty in control due to line and point contacts. A smaller flat area may also lead to difficulty in maintaining balance. These control issues, as well as extension to three-dimensional shapes, should be studied in order to evaluate the practical applicability of such feet to real robots.

ACKNOWLEDGEMENTS

The authors would like to thank Jessica Hodgins for providing the research environment and Ronit Slyper for giving comments on the paper.

REFERENCES

[1] H. Hirukawa, S. Hattori, S. Kajita, K. Harada, K. Kaneko, F. Kanehiro, M. Morisawa, and S. Nakaoka, "A pattern generator of humanoid

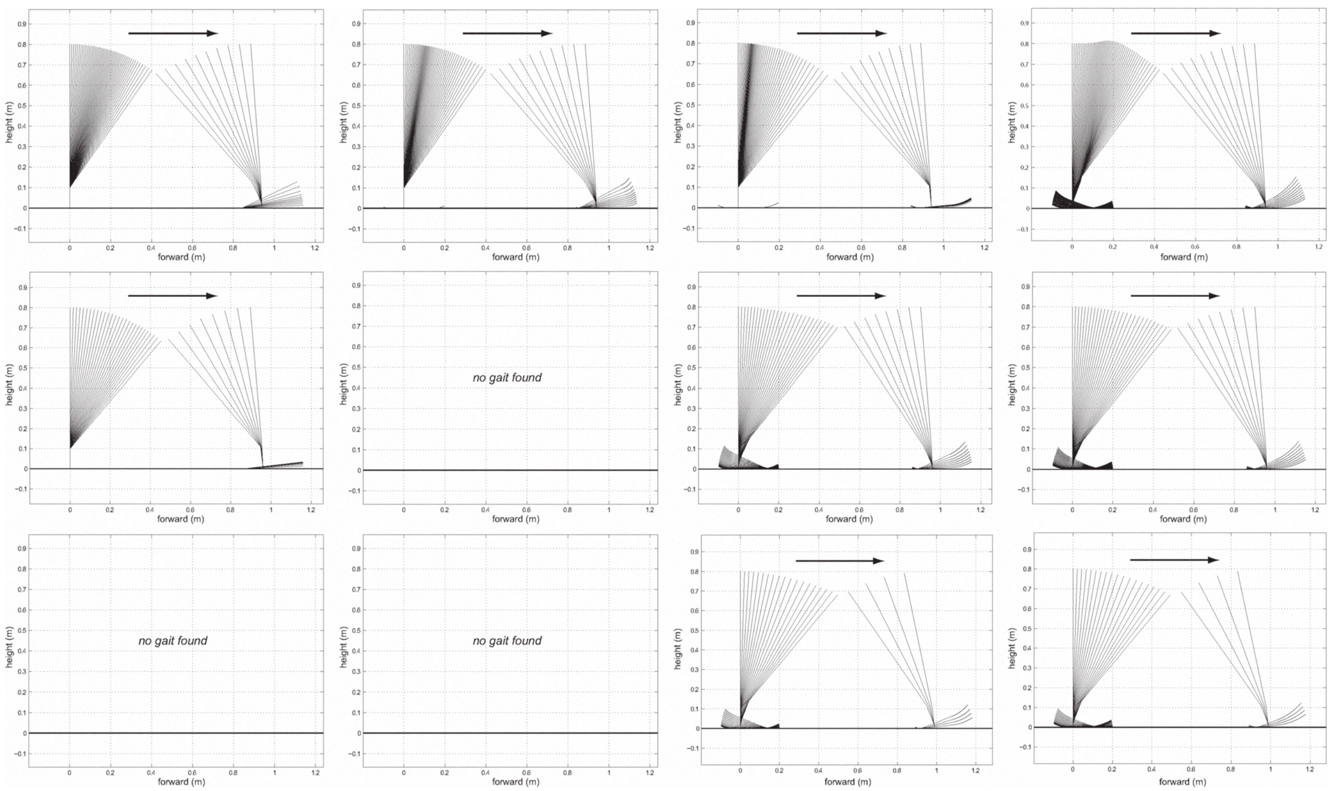

Fig. 5. Optimized gaits. From top to bottom row: slow, normal, and fast walk. From left to right column: *Flat*, *Curved 1*, *Curved 2* and *Curved 3*.

robots walking on a rough terrain," in *Proceedings of IEEE International Conference on Robotics and Automation*, 2007, pp. 2181–2187.

[2] J.-S. Gutmann, M. Fukuchi, and M. Fujita, "Stair climbing for humanoid robots using stereo vision," in *Proceedings of IEEE/RSJ International Conference on Intelligent Robots and Systems*, 2004, pp. 1407–1413.

[3] T. McGeer, "Passive dynamic walking," *International Journal of Robotics Research*, vol. 9, no. 2, pp. 62–82, 1990.

[4] K. Hirai, M. Hirose, Y. Haikawa, and T. Takenaka, "The development of honda humanoid robot," in *Proceedings of IEEE International Conference on Robotics and Automation*, vol. 2, May 1998, pp. 1321–1326.

[5] T. Ishida, "Development of a small biped entertainment robot qrio," in *Proceedings of the 2004 International Symposium on Micro-Nanomechatronics for Information-Based Society*, Oct.-3 Nov. 2004, pp. 23–28.

[6] Y. Ogura, H. Aikawa, K. Shimomura, A. Morishima, H. ok Lim, and A. Takanishi, "Development of a new humanoid robot wabian-2," in *Proceedings of IEEE International Conference on Robotics and Automation*, May 2006, pp. 76–81.

[7] K. Nishiwaki, J. Kuffner, S. Kagami, M. Inaba, and H. Inoue, "The experimental humanoid robot H7: a research platform for autonomous behaviour," *Royal Society of London Philosophical Transactions Series A*, vol. 365, pp. 79–107, Jan. 2007.

[8] S. Lohmeier, T. Buschmann, H. Ulbrich, and F. Pfeiffer, "Modular joint design for performance enhanced humanoid robot lola," in *Proceedings of IEEE International Conference on Robotics and Automation*, May 2006, pp. 88–93.

[9] A. Konno, R. Sellaouti, F. Amar, and F. Ouezdou, "Design and development of the biped prototype robian," in *Proceedings of IEEE International Conference on Robotics and Automation*, vol. 2, 2002, pp. 1384–1389 vol.2.

[10] R. Sellaouti, O. Stasse, S. Kajita, K. Yokoi, and A. Kheddar, "Faster and smoother walking of humanoid hrp-2 with passive toe joints," in *Proceedings of IEEE/RSJ International Conference on Intelligent Robots and Systems*, Oct. 2006, pp. 4909–4914.

[11] Y. Ogura, K. Shimomura, H. Kondo, A. Morishima, T. Okubo, S. Momoki, H. Lim, and A. Takanishi, "Human-like walking with knee stretched, heel-contact and toe-off motion by a humanoid robot," in *Proceedings of IEEE/RSJ International Conference on Intelligent Robots and Systems*, 2006, pp. 3976–3981.

[12] F. Ouezdou, S. Alfayad, and B. Almasri, "Comparison of several kinds of feet for humanoid robot," in *Proceedings of the 5th IEEE-RAS International Conference on Humanoid Robots*, Dec. 2005, pp. 123–128.

[13] M. Nishikawa et al., "Foot structure for legged walking robot," United States Patent No. 5,255,753, 1993.

[14] P. G. Adamczyk, S. H. Collins, and A. D. Kuo, "The advantages of a rolling foot in human walking," *J Exp Biol*, vol. 209, no. 20, pp. 3953–3963, 2006. [Online]. Available: http://jeb.biologists.org/cgi/content/abstract/209/20/3953

[15] S. H. Collins, M. Wisse, and A. Ruina, "A three-dimensional passive-dynamic walking robot with two legs and knees," *I. J. Robotic Res.*, vol. 20, no. 7, pp. 607–615, 2001.

[16] M. Wisse, D. Hobbelen, R. Rottevell, S. Anderson, and G. Zeglin, "Ankle springs instead of arc-shaped feet for passive dynamic walking," in *Proceedings of the 6th IEEE-RAS International Conference on Humanoid Robots*, November 2006, pp. 110–116.

[17] M. Garcia, A. Chatterjee, A. Ruina, and M. Coleman, "The simplest walking model: Stability, complexity, and scaling," *ASME Journal of Biomechanical Engineering*, vol. 120, pp. 281–288, 1998.

[18] "CMU graphics lab motion capture database," http://mocap.cs.cmu.edu/.

[19] D. A. Winter, *Biomechanics and Motor Control of Human Movement*, 4th ed. Hoboken, NJ: John Wiley & Sons, 2009.